Evaluating the Antifouling Properties of Poly(ether sulfone)/Sulfonated Poly(ether sulfone) Blend Membranes in a Full-Size Membrane Module

Fang, Li-Feng ; Kato, Noriaki ; Yang, Hui-Yan ; Cheng, Liang ; Hasegawa, Susumu ; Jeon, Sungil ; Matsuyama, Hideto

(Citation)
Industrial & Engineering Chemistry Research,57(12):4430-4441

(Issue Date)
2018-03-28

(Resource Type)
journal article

(Version)
Version of Record

(URL)
https://hdl.handle.net/20.500.14094/90004931

I&EC research
Industrial & Engineering Chemistry Research

Article

Cite This: Ind. Eng. Chem. Res. 2018, 57, 4430−4441

pubs.acs.org/IECR

Evaluating the Antifouling Properties of Poly(ether sulfone)/Sulfonated Poly(ether sulfone) Blend Membranes in a Full-Size Membrane Module

Li-Feng Fang, Noriaki Kato, Hui-Yan Yang, Liang Cheng, Susumu Hasegawa, Sungil Jeon, and Hideto Matsuyama*

Center for Membrane and Film Technology, Department of Chemical Science and Engineering, Kobe University, Rokkodaicho 1-1, Nada, Kobe 657-8501, Japan

Supporting Information

ABSTRACT: To evaluate the antifouling properties of the poly(ether sulfone) (PES)/sulfonated poly(ether sulfone) (SPES) blend membranes, the full-size membrane modules containing pure PES hollow fiber membranes and PES/SPES blend hollow fiber membranes were prepared and compared. First, a series of PES/SPES blend hollow fiber membranes with different SPES fraction were fabricated by a nonsolvent-induced phase separation (NIPS) process. The surface chemical compositions, morphology, surface wettability, permeability, and mechanical strength of the membranes were characterized. After assembling the module, the permeability and antifouling properties of the full-size modules were tested in a lab-scale evaluation system. Each full-size membrane module in this study included approximately 330 pieces of 1 m long hollow fiber membranes with an effective area of approximately 1 m^2. Three model foulants, i.e., sodium alginate (SA), humic acid (HA), and bovine serum albumin (BSA), and three real river water samples were used in evaluation of the antifouling properties. Hermia's models adapted to cross-flow ultrafiltration were used to investigate the fouling mechanism involved in the ultrafiltration of SA, HA, BSA, and river water samples. The results indicated that the membrane module containing the hollow fiber membranes with 10% of SPES (MD20-10) showed better antifouling properties than the membrane module containing pure PES hollow fiber membranes (MD22-0). In addition, the main fouling mechanism for all foulant is the complete blocking, intermediate blocking, or gel layer formation. Moreover, it was also confirmed that module MD20-10 possessed a sufficient chemical cleaning capability, which implied a promising potential for its practical application.

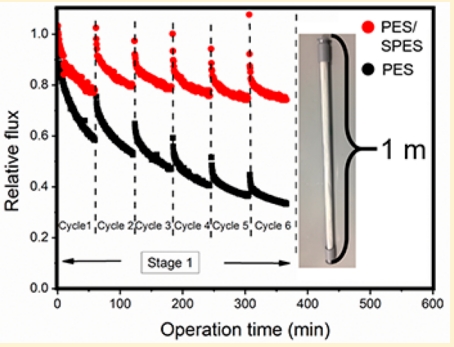

1. INTRODUCTION

Nowadays, amphiphilic copolymers are attracting a great deal of attention for fabrication and modification of polymeric membranes.[1−4] Among them, sulfonated poly(ether sulfone) (SPES) is considered as an effective membrane additive/material applied for various applications, including water treatment,[5−8] gas separation,[9,10] energy production,[11−16] and catalytic membrane fabrication.[17,18]

Because of the hydrophilic and negatively charged sulfonate groups on the poly(ether sulfone) (PES) backbones, SPES is often used to prepare antifouling ultrafiltration membranes.[19] The hydrated layer formed on the hydrophilic surface creates a physical/chemical barrier that prevents foulants from approaching the hydrophobic matrix. On the other hand, an electrostatic repulsion occurs between the negatively charged surface and the negatively charged foulants. Kim et al.[7] proved that SPES reduced bovine serum albumin (BSA) fouling at a wide range of pH (3.0−8.0). Wang et al.[20] testified that a PES/SPES blend membrane reduced BSA adsorption and prolonged the blood coagulation time compared with a neat PES membrane, indicating the promising application for hemodialysis and blood purification. Li and Chung[21] reported a dual-layer hollow fiber membrane made from SPES with durable protein separation performance, which was attributed to the strong electrostatic attraction of hemoglobin molecules (a kind of positively charged protein) and to the shielding effect caused by the adsorbed molecules for BSA diffusion. Moreover, the negatively charged surface also generates an interaction force with cations, which are further immobilized onto the surface. For instance, silver particles were immobilized onto SPES membranes, thus achieving the antibacterial capacity.[22] Therefore, SPES is an effective membrane material and additive, and PES/SPES blend membrane is a type of hydrophilic membrane with high performance.

Although there are so many publications reporting the improved properties of membranes by the polymer blending method, most of them are limited to fundamental studies.

Received: January 8, 2018
Revised: March 1, 2018
Accepted: March 1, 2018
Published: March 1, 2018

DOI: 10.1021/acs.iecr.8b00114
Ind. Eng. Chem. Res. 2018, 57, 4430−4441

Table 1. Characteristic Properties of Pure PES Hollow Fiber Membranes and PES/SPES Blend Hollow Fiber Membranes

membrane ID	o.d. (μm)	i.d. (μm)	wall thickness (μm)	pure water perm. (L m^{-2} h^{-1} bar^{-1})	tensile strength (MPa)	elongation (%)	Young modulus (MPa)	air bubble contact angle[a] (deg)
M20-0	985	784	100	350	7.1	98	0.18	118
M22-0	881	643	119	159	9.8	118	0.22	117
M20-5	1001	762	120	157	5.1	71	0.12	125
M20-10	948	655	147	146	4.1	66	0.09	134
M23-30	1021	728	146	41	2.7	44	0.05	134

[a]The air bubble contact angle was tested on the flat sheet membrane with the same composition.

Compared with the flat sheet membranes, hollow fiber membranes have been widely used in the field of water treatment due to their high packing density, small footprint, and high filtration efficiency.[23,24] The performance of the hollow fiber membranes is usually evaluated with a small-size hollow fiber membrane module containing 1−10 fibers with the length of 6−25 cm (Table S1, please refer to Supporting Information).[25−31] Obviously, such evaluation modules are much smaller than those used commercially.[32] Therefore, it is critical to evaluate the membrane properties in commercially sized modules for further scaling-up of water treatment processes.

In this work, antifouling properties of the full-size membrane modules were evaluated using several types of PES-related hollow fiber membranes, i.e., pure PES membranes and PES/SPES blend membranes. First, the membranes were prepared by a traditional nonsolvent-induced phase separation process, and then the single hollow fibers were characterized. After that, several full-size modules containing pure PES membranes and PES/SPES blend membranes were fabricated. In the modules, there were about ∼330 pieces of hollow fiber with a length of 1.0 m. Model foulants, such as sodium alginate (SA), humic acid (HA), and BSA, were chosen for antifouling evaluation. Furthermore, several real river water samples were also collected and used to evaluate the antifouling properties of the modules. Furthermore, Hermia's models adapted to cross-flow ultrafiltration[33,34] were used to investigate the fouling mechanism involved in the ultratfiltration of SA, HA, BSA, and river water samples. We expect that this study provides the helpful guidance for the antifouling evaluation on the full-size modules containing blend membranes.

2. EXPERIMENTAL SECTION

2.1. Materials and Reagents. Poly(ether sulfone) (PES, Ultrason E6020P, M_w = 58 000 g mol^{-1}) was obtained from BASF Co., USA. Sulfonated poly(ether sulfone) (SPES1#, M_w = 110 000 g mol^{-1}, degree of sulfonation (DS) = 30%; SPES2#, M_w = 141 000 g mol^{-1}, DS = 30%) was kindly supplied by Konishi Chemical Ind. Co., LTD, Japan. Dimethylacetamide (DMAc) and bovine serum albumin (BSA) were purchased from Wako Pure Chemical Industries, Japan. Sodium alginate (SA) was obtained from Aldrich Chemical Co., USA. Humic acid (HA) was obtained from Sigma-Aldrich Chemie GmbH, Germany.

Three river water samples (Yodo River, Kako River, and Seta River) were collected in the autumn of 2016. Detailed information on these river samples is listed in Table S2. The quality of the river water samples was characterized by the total organic carbon analyzer (TOC, TOC-VCSH, Shimadzu Co., Japan), liquid chromatogram−organic carbon detector (LC-OCD, Model 8, DOC-Labor, Germany), and excitation−emission matrix fluorescence spectroscopy (EEM, Aqualog, HORIBA, Ltd., Japan). In LC-OCD results, DOC represents the dissolved organic carbon. Biopolymer represents polysaccharides with higher molecular weight, >50 000−2 000 000 g mol^{-1}. Humics represent consists of humic acids and fulvic acid in varying amounts. Building blocks represent humics−hydrolysates, intermediates in the degradation process. Neutrals represent slightly hydrophobic substances, such as alcohols, aldehydes, ketones, and amino acids. Acids represent final degradation products of organics, but also released by algae and bacteria.[35] In EEM results, the NOM is mainly divided into five regions, that is, regions I−V, referring to aromatic protein I, aromatic protein II, fulvic acid-like, soluble microbial byproduct-like, and humic acid-like in water, respectively.[36]

2.2. Fabrication of Hollow Fiber Membranes. The hollow fiber membranes were prepared using a hollow fiber spinning machine consisting of a dope dissolving unit, a spinneret unit, a coagulation bath unit, and a winding unit, by the nonsolvent-induced phase separation (NIPS) method. The compositions of the casting solutions are listed in Table S3. The homogeneous dope solution (40 °C) was extruded though a spinneret (inner diameter, 0.5 mm; outer diameter, 1.3 mm; referring to Figure S1) with an inner lumen made by a bore liquid (Milli-Q water) into a coagulation bath (water, 40 °C), in which phase separation and solidification took place. The gap between the spinneret and the coagulation bath was 12.5 cm, and the hollow fiber was wound on a take-up winder at ∼11 m min^{-1}. The wound fibers were cut into bundles of ∼100 fibers with 1.5 m in length. The residual solvent in the prepared membrane was extracted using excess amounts of water. Finally, the hollow fiber membrane bundles were soaked in a 60 wt % glycerol solution for at least 72 h and dried at 50 °C thereafter. The detailed information on hollow fiber membranes before glycerol soaking and drying is listed in Table 1.

2.3. Characterizations of Hollow Fiber Membranes. The shape and size of the hollow fiber membranes were observed with an optical microscope (SKM-S30C, Saito Kogaku Co., Japan), connected to a computer. The images were recorded and analyzed directly from live video (software: SK-Viewer, Saito Kogaku Co., Japan). The water permeability of the hollow fiber membrane was measured using a homemade module that comprise a single hollow fiber membrane. The effective length inside the module was 240 mm. The mechanical strength of the hollow fiber membranes was determined by a tensile strength tester (AGS-J, Shimadzu Co., Japan). The length of each samples was 5 cm, and the stretching rate was 50 mm min^{-1}. Every value obtained was averaged from at least six parallel samples. The membrane morphology was observed by scanning electron microscope (SEM, JSF-7500F, JEOL, Japan). The cross sections of the fibers were obtained by fracturing them in liquid nitrogen. All the surfaces and cross sections were coated with a thin osmium oxide layer using an osmium coater (Neoc-STB, MEIWAFOSIS Co. Ltd., Japan) before SEM observation. The surface chemical compositions of the membranes were characterized by X-ray photoelectron spectroscopy (XPS, JSP-

DOI: 10.1021/acs.iecr.8b00114
Ind. Eng. Chem. Res. 2018, 57, 4430−4441

9010MC, JEOL, Japan) with Al Kα excitation radiation (1486.6 eV). For these measurements, 5−6 pieces of the hollow fiber membranes (approximately 6 mm in length) were attached onto a carbon tape together to achieve an effective area of approximately 6 mm × 6 mm. The binding energy was calibrated by the existing C 1s (285 eV). The surface hydrophilicity of the membranes was measured by the air bubble contact angle on a contact angle goniometer (Drop Master 300, Kyowa Interface Science Co., Japan). The air bubble contact angle is defined as the angle from the solid surface to the air−water interface through the air phase.

2.4. Preparation of the Full-Size Membrane Module. The dried bundles of the hollow fiber membranes were placed into a module with a length of 1 m, each of which contained approximately 330 pieces of fibers. In this case, the outer membrane area was approximately 1 m^2. Potting of the module end portion was carried out with a urethane resin using a normal centrifugation method. The module was designed to be an "out to in" filtration type, and the hollow fibers were open only at one end. Therefore, the module had three ports: an inlet and an outlet for the feed liquid passing along the exterior of the hollow fibers and an outlet for the permeate solution at the open end of the hollow fibers. The feed inlet was at the same side as the closed end of the hollow fiber and the feed and permeate were in parallel flow. Figure 1 shows the appearance of the full-size membrane module used in this study.

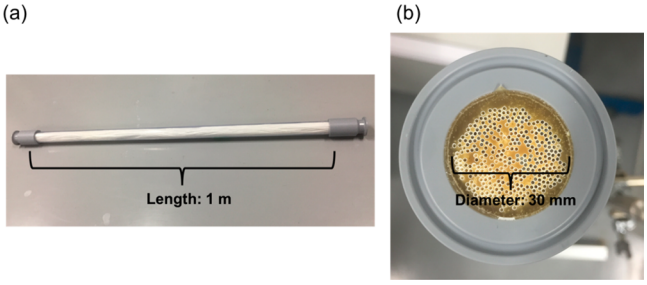

Figure 1. (a) Photo of a full-size membrane module with a length of 1 m. (b) Outlet for the permeate solution of a membrane module.

2.5. Module Evaluation. The permeability and antifouling properties of the full-size modules were tested on a lab-scale evaluation system (Microza LX-22001, Asahi Kasei Chem. Co., Japan), the schematic diagram of which is shown in Figure 2. The procedure is as follows. Before the fouling measurement, the water permeability was measured with tap water. The pressure at the inlet (P_{in}, bar) was set at 30−50 kPa for different modules to obtain the similar water flux (J_w, L m^{-2} h^{-1}). The water permeability (L m^{-2} h^{-1} bar^{-1}) of the module was obtained according to following equation:

$$\text{water permeability} = \frac{J_w}{(P_{in} + P_{out})/2} \quad (1)$$

where P_{out} is the pressure at the outlet.

The fouling measurement included three stages. In the first stage, 30 L of foulant solution was used as the feed solution in the circulation. In addition, a 10-fold concentration of foulant solution was continuously injected to the feed solution tank to keep the foulant concentration. The filtration process was operated at the constant inlet pressure for 1 h. Then the rinsing process was carried out. The module was backflushed under 40 kPa for 30 s with clean tap water, and then it was aerated for 10 s with an air flow rate of 2.5 L min^{-1}. Subsequently, the residual solution (approximately 1.2 L) was discharged. In the following 5 h, the filtration and rinsing process was repeated for five times. Here, 1 h filtration process and one time rinsing process are defined as one cycle. Therefore, six cycles were completed in the first stage.

In the second stage, the membrane module was thoroughly rinsed by clean tap water using the following procedure. First, the solution in the feed solution tank was completely replaced with clean tap water. Then, the whole system was circulated with clean tap water with a flow rate of 50 L min^{-1} for 3−5 min, after which the module was backflushed for 1 min and aerated for 30 s. The system was then rinsed for 1 min. Subsequently, the solution in the tank was replaced with clean tap water again, and the previous process was repeated once more. Finally, the clean tap water flux was measured again at the same inlet pressure. In the third stage, the membrane module was taken out of the evaluation system and soaked in a chemical solution containing 1000 ppm of NaClO and 1 mM NaOH for 3 days. Lastly, the clean tap water flux after the chemical cleaning was measured again using the same conditions in the evaluation system.

The rejections (R, %) for HA and BSA of membrane modules are calculated according to the following equation:

$$R = \left(1 - \frac{c_p}{c_f}\right) \times 100\% \quad (2)$$

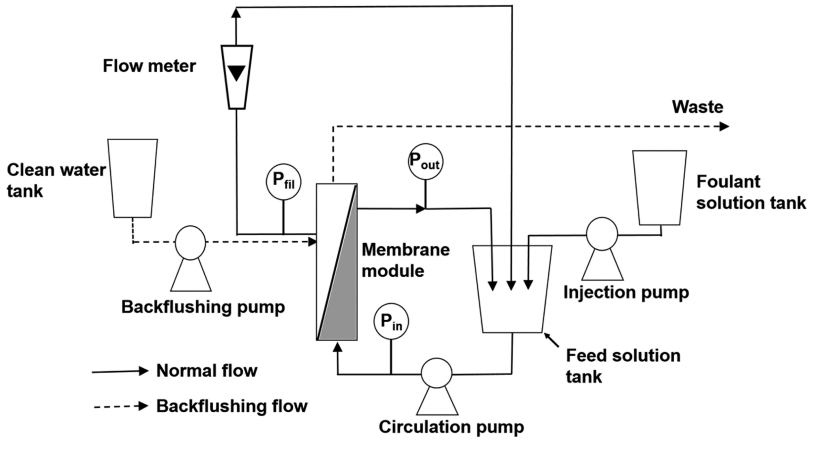

Figure 2. Schematic diagram of the evaluation system of the full-size membrane module.

DOI: 10.1021/acs.iecr.8b00114
Ind. Eng. Chem. Res. 2018, 57, 4430−4441

where c_f and c_p refer to the concentrations of feed and permeate solutions, respectively. HA and BSA concentrations were determined by the total organic carbon analyzer (TOC, TOC-VCSH, Shimadzu Co., Japan) and UV−vis spectroscopy (U-2000, Hitachi Co., Tokyo, Japan) at a wavelength of 280 nm, respectively.

3. RESULTS AND DISCUSSION

3.1. Characterizations of Single Hollow Fiber Membranes. Five different membranes were prepared by the NIPS method: two pure PES membranes (M20-0 and M22-0) and three PES/SPES blend membranes (M20-5, M20-10, and M23-30). The characteristic properties, morphology, and surface chemical compositions of the prepared membranes were characterized, and the results are shown in Tables 1 and 2 and Figure 3. For the pure PES membranes, the membrane with higher polymer concentration, i.e., M22-0, exhibits a higher membrane thickness, lower water permeability, and higher mechanical strength than M20-0. As for the PES/SPES blend membranes, their membrane thickness is higher than that of the pure PES membranes due to the pore forming effect of SPES during the phase separation process. Because of the higher affinity between SPES and coagulation bath, the polymer-rich rich and polymer-lean phases can tolerate more content of water before gel formation, leading to larger pore sizes in the matrix and larger porosity.[4,37] To obtain a similar permeability, the polymer concentration with different SPES fractions is slightly changed. When doping a low fraction of SPES (M22-0, M20-5, and M20-10), these membranes show a similar water permeability (approximately 150 L m^{-2} h^{-1} bar^{-1}, wet membranes before glycerol drying). These membranes with similar water permeability are suitable for the fouling experiments because the water permeability effect is eliminated, and the effect of pure membrane material can be evaluated in isolation. On the other hand, the permeability sharply decreases for M23-30 (Table 1). This is mainly caused by the increase in the thickness of the spongelike sublayers in both inner and outer surfaces (Figure 3), which dramatically increases the water diffusion resistance.[38,39] The most critical problem for M23-30 that deserves attention is its low mechanical strength compared with the other membranes, which represents ∼38% of the mechanical strength of M20-0 and ∼28% of that of M22-0. Because of the flexibility of the sulfonate group and the water adsorption capability of the hydrophilic segments of SPES, the tensile strength, the elongation at break, and the Young modulus of a single hollow fiber decrease with an increase of the SPES fraction in the polymer blend. Therefore, it is impossible to make a membrane with higher permeability than that of M23-30 by decreasing the polymer concentration because it would result in a fiber too weak to fabricate by the spinning method.

Table 2. Chemical Compositions of the Outer Surfaces of the Membranes

membrane ID	C (%)	O (%)	S (%)
M20-0/M22-0	70.4	22.8	6.8
M20-5	73.1	21.4	5.5
M20-10	72.4	20.1	7.5
M23-30	73.2	19.9	6.9

The air bubble contact angle was used to confirm the hydrophilicity of the blend membranes, and the higher one represents the better hydrophilicity.[4] It is found that PES/SPES blend membranes show the higher contact angles (Table 1), indicating that the surface hydrophilicity of blend membranes is enhanced compared with the pure PES membranes.

The membrane morphology was characterized by an optical microscope and a scanning electron microscope (SEM). As shown in Figure 3a, the cross-sectional shapes of M20-0, M22-0, M20-5, and M20-10 are regular circular rings with uniform thickness due to their sufficient mechanical strength. However, in the case of M23-30, the membrane thickness visible in the cross sections is not uniform, which is mainly due to the weak mechanical strength of this membrane. Double finger-like structures can be observed at the cross sections near the inner and outer layers in Figure 3b because water is used for both the coagulation bath and bore flow. An instantaneous phase separation occurs when the extruded fiber is immersed in water, resulting in porous structures. Because of the hydrophilicity of SPES, the casting solution containing PES/SPES blend can accommodate more water before gelation and solidification occurs, which results in a delayed phase separation and thus an increased thickness of sponge-like sublayers in both inner and outer surfaces of M23-30.[19] However, the investigation on detailed phase separation mechanism is still on the way and will be presented in our following research article. As for the surfaces of all membranes, both the inner and outer surfaces visually reveal the absence of pores, which is in accordance with a previous study.[5]

The XPS results show the similar surface chemical compositions on the outer surfaces of the pure PES and blend membranes (Table 2). If the hydrophilic part of SPES segregates on the membrane surface, the amount of oxygen increases. The results of Table 2 indicate no apparent surface segregation phenomenon of hydrophilic SPES is observed, which is in contrast with our previous studies.[4,40] This is mainly attributed to the rigid structures of hydrophilic sulfonated groups when they directly covalently bond with benzene rings and limitation of the chemical segregation onto the uppermost surface during the phase separation process.[19]

In summary, several kinds of pure PES hollow fiber membranes and PES/SPES hollow fiber membranes with different SPES fractions were successfully fabricated and subsequently used for module preparation and evaluation.

3.2. Characterizations and Antifouling Properties Evaluation of Full-Size Membrane Modules. *3.2.1. Characteristics of Full-Size Membrane Modules.* Because of the low mechanical strength of M23-30, these fibers cannot be made into the module. The detailed information on the full-size membrane modules with other four types of membranes, namely M20-0, M22-0, M20-5, and M20-10, are listed in Table 3. Compared with the membrane sizes shown in Table 1, the shapes and sizes of the hollow fibers before and after glycerol-drying process are similar. However, the water permeability for M20-10 is noticeably lower compared with the other fibers. This is mainly caused by the shrinkage of the hydrophilic matrix during the drying process. The prepared modules are denoted as MD22-0, MD20-0, MD20-5, and MD20-10, corresponding to the inset hollow fibers (M22-0, M20-0, M20-5, and M20-10, respectively). According to their final pure water permeability of the modules, the modules are divided into two groups with similar water permeability, that is, MD20-0 and MD20-5 and MD22-0 and MD20-10. Moreover, MD22-0 and MD20-10 have the similar rejections of HA and BSA.

3.2.2. Effect of SPES Fraction on the Antifouling Properties of Full-Size Membrane Modules. In order to eliminate the

DOI: 10.1021/acs.iecr.8b00114
Ind. Eng. Chem. Res. 2018, 57, 4430−4441

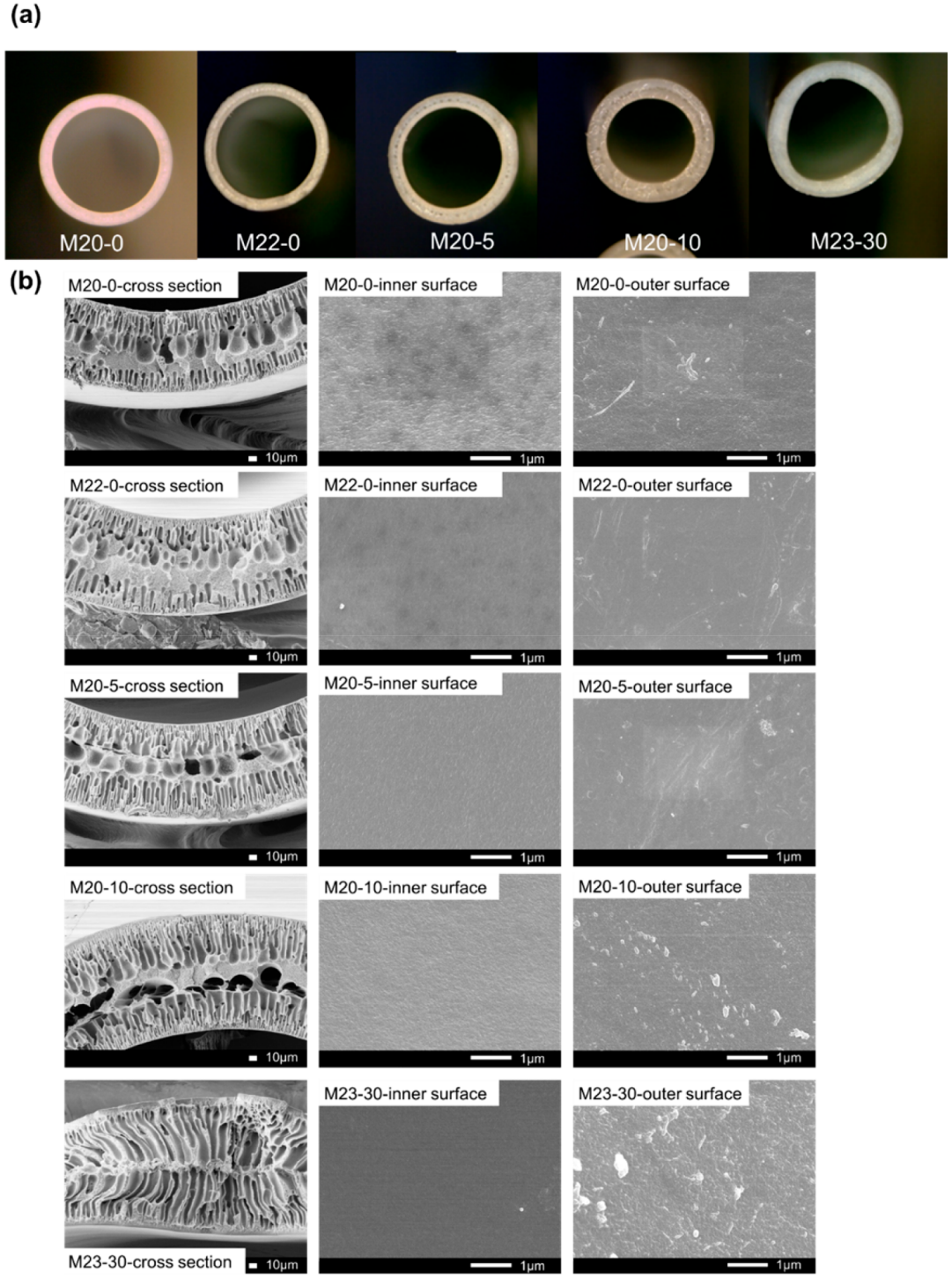

Figure 3. Morphology of pure PES hollow fiber membranes (M20-0 and M22-0) and PES/SPES blend hollow fiber membranes (M20-5, M20-10, and M23-30): (a) optical microscope photographs; (b) SEM images.

hydraulic effect during the fouling measurement,[4] the initial flux for each group was adjusted to the same level by changing the operation pressure. For MD20-0 and MD20-5, the initial water flux was approximately 40 L m^{-2} h^{-1}, while for MD22-0 and MD20-10, the initial water flux was approximately 22 L m^{-2} h^{-1}. As shown in Figure 4a, the fluxes of M22-0 and M20-5 sharply decrease when the feed solution is changed to SA solution. Here, we define the ratio of the flux after 1 h SA fouling experiment to the initial flux as flux retention (FR, %) and the ratio of the flux after the rinsing process and the initial flux as flux recovery ratio (FRR, %). Higher values of FR and FRR mean the better antifouling properties. It is observed that FR values for MD20-0 and MD20-5 after six-cycle operation are 15.3% and 21.7%, respectively (Figure 4c), indicating the severe membrane fouling. After five cycles, FRR values for M20-0 and M20-5 are ∼38%, implying that most membrane fouling is irreversible fouling,[4,41] which are mainly attributed to the hydrophobic interaction between the foulant and the membrane matrix. After thoroughly rinsing with clean water (stage 2 in Figure 4a), the stable recovered water fluxes for both modules are similar, around 40%

DOI: 10.1021/acs.iecr.8b00114
Ind. Eng. Chem. Res. 2018, 57, 4430−4441

Table 3. Summary Information of the Membrane Modules

	single hollow fiber membrane after glycerol-drying process			characteristics of membrane modules					performance of fresh membrane modules		
module ID	o.d. (μm)	i.d. (μm)	wall thickness (μm)	fiber no.	outer surface area (m^2)	length (m)	i.d. (mm)	packing density (%)	water permeability (L m^{-2} h^{-1} bar^{-1})	rejection of HA (%)	rejection of BSA (%)
MD20-0	944	744	100	340	1.008	1	30	33.6	176		
MD22-0	885	647	117	346	0.957	1	30	29.5	102	87	81
MD20-5	1015	755	120	285	0.910	1	30	32.6	187		
MD20-10	872	547	162	299	0.819	1	30	25.3	56	85	78

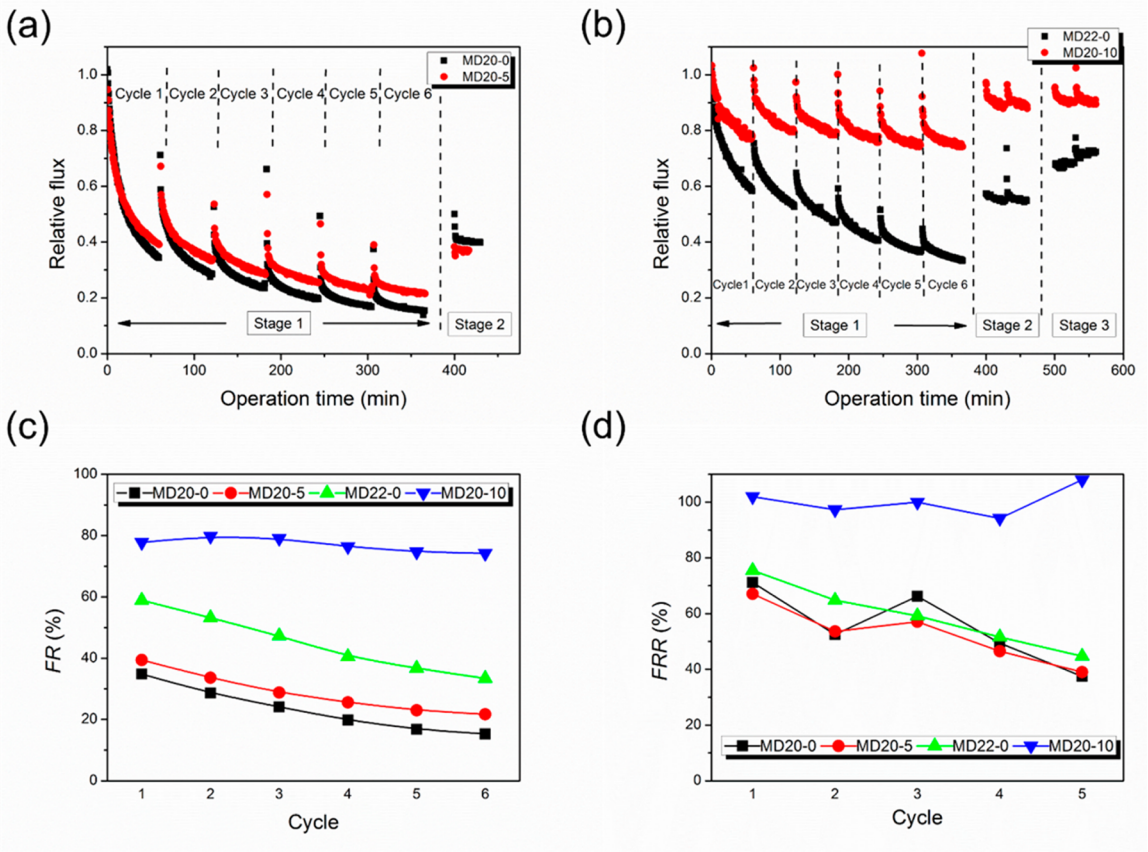

Figure 4. Effect of the SPES fraction in the polymer blend on the antifouling properties of full-size membrane modules: (a) relative fluxes of MD20-0 and MD20-5 vs operation time, including two stages; (b) relative fluxes of MD22-0 and MD20-10 vs operation time, including three stages; (c) flux retention (FR) after 1 h fouling vs cycles; (d) flux recovery ratio (FRR) after rinsing process vs cycles. A 100 ppm of SA solution was chosen as the foulant.

of the initial water flux. Therefore, 5% of SPES fraction in the polymer blend cannot effectively mitigate membrane fouling.

Considering MD22-0 and MD20-10, the flux decrease during the fouling process for MD20-10 was obviously much lower when compared with that for MD22-0 (Figure 4b). The FR value kept at 0.742 after six-cycle operation for MD20-10, while that of MD22-0 was kept at 0.334 (Figure 4c). It should be mentioned that the FR values were almost the same (approximately 77%) for each of the six cycles of the fouling process for MD20-10, while for MD22-0, the FR value after the sixth cycle (approximately 33%) is nearly half of that after the first cycle (approximately 59%). These results strongly prove that MD20-10 shows the durable antifouling properties during a multiple cycle operation, whereas the membrane fouling on MD22-0 becomes increasingly severe. The FRR values (Figure 4d) also give the evidence of the excellent antifouling properties of MD20-10. Furthermore, the stable fluxes of MD22-0 and MD20-10 in stage 2 are ~56% and ~90% of the initial water flux, respectively. The improved hydrophilicity (Table 1) and endowed negative charge[21] of the PES/SPES membrane obviously reduce the foulant deposition on the membrane surface and pores, and the attached foulant is easily washed away from this membrane by simple water flushing.

3.2.3. Effect of Types of Model Foulants on the Antifouling Properties of Full-Size Membrane Modules. With our previous results, only modules (MD22-0 and MD20-10) were further used in our evaluation of the membrane antifouling properties. Typical model foulants (HA and BSA) were used to evaluate the membrane antifouling properties. During the HA fouling measurement, the procedure is slightly different from the previous one: during stage 1, two modules were operated under the same pressure (25 kPa) in first three cycles (0−180 min); then they were operated under the same flux (25 kPa for MD22-0 and 44 KPa for MD20-10) in the following three cycles (181−360 min). As shown in Figure 5a, the flux decay for MD22-0 is more severe than that for MD20-10 during the fouling measurement in stage 1. After each rinsing process, the flux

DOI: 10.1021/acs.iecr.8b00114
Ind. Eng. Chem. Res. 2018, 57, 4430−4441

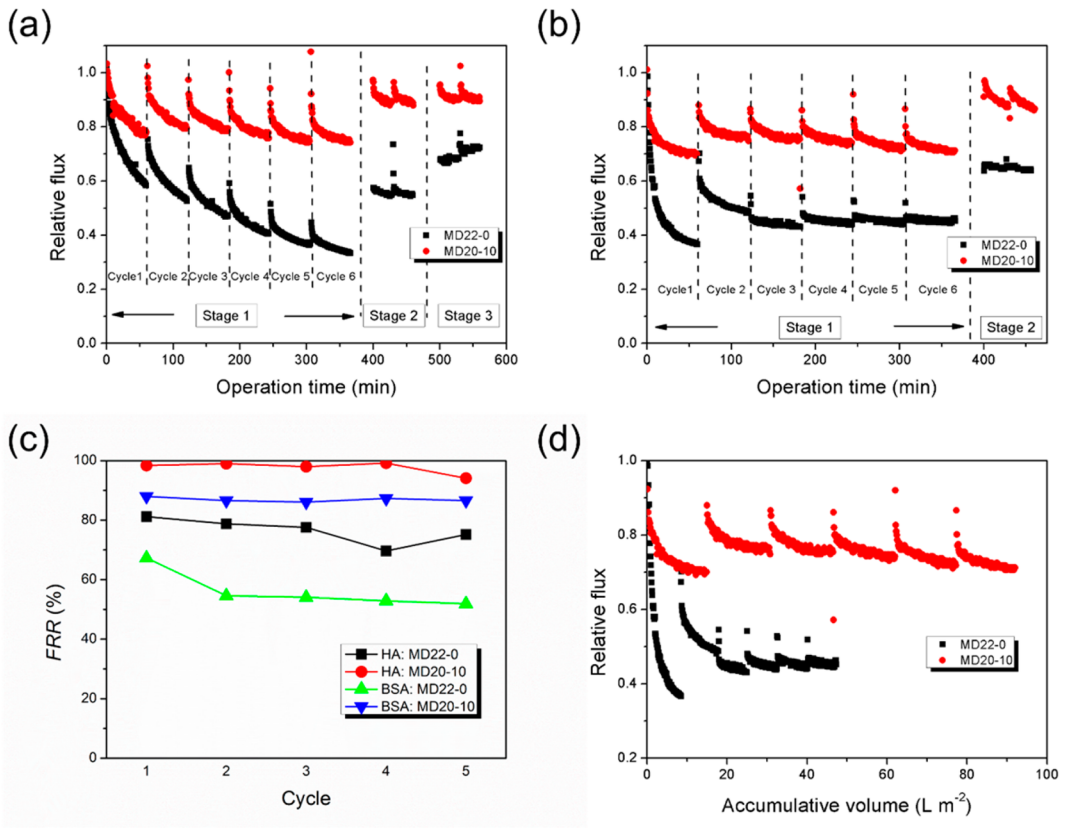

Figure 5. Effect of different model foulants (HA and BSA) on the antifouling properties of full-size membrane modules: (a) relative flux vs operation time, using 100 ppm of HA solution as the foulant; (b) relative flux vs operation time, using 100 ppm BSA solution as the foulant; (c) flux recovery ratio (FRR) after rinsing process vs cycles, using 100 ppm of HA and 100 ppm BSA solutions as the foulants; and (d) relative flux vs accumulative volume, using 100 ppm BSA solution as the foulant.

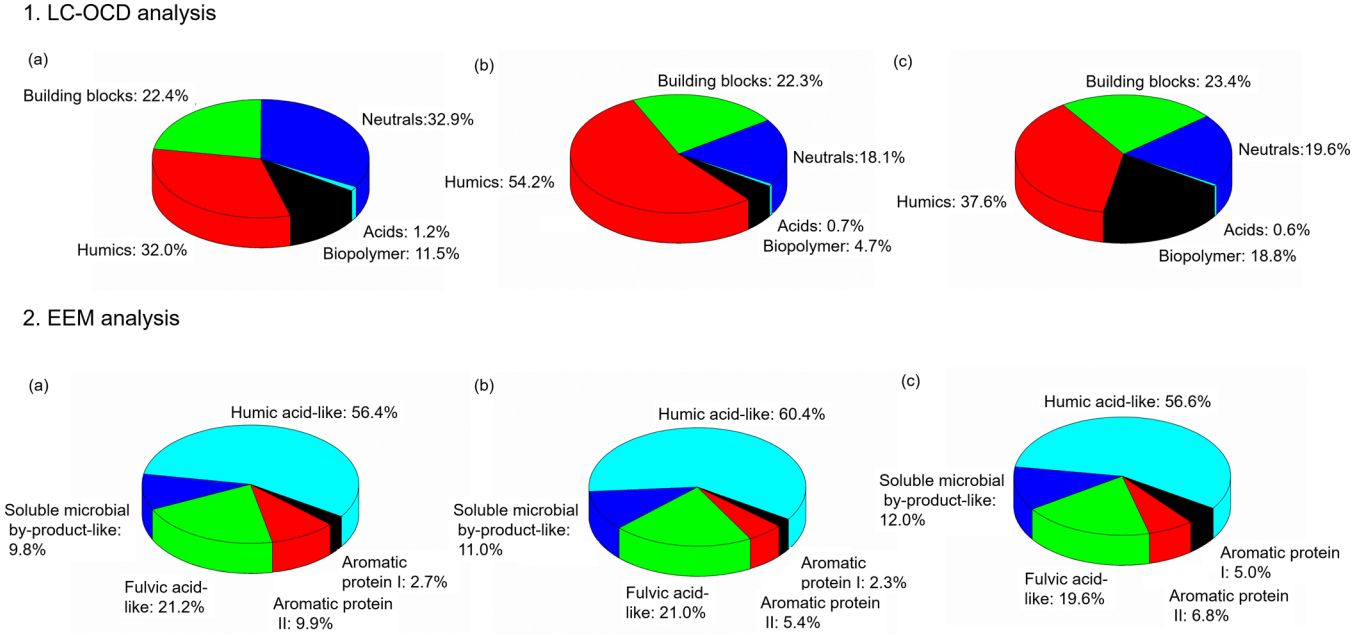

Figure 6. Detailed fractions of the natural organic matter (NOM) in river water samples (a, Yodo River; b, Kako River; c, Seta River) by (1) LC-OCD analysis and (2) EEM analysis.

recovery ratios (FRRs) in five cycles are higher than 94% for MD20-10, but they gradually decrease from 81% to 75% for MD22-0 (Figure 5c), indicating that increasingly more foulants are deposited on the membrane after five filtration−rinsing cycles. FRRs for MD20-10 and MD22-0 in stage 2 are 96% and 73%, respectively, which implies that HA attached on PES/SPES membranes is easily washed away by simple backflushing process.

DOI: 10.1021/acs.iecr.8b00114
Ind. Eng. Chem. Res. 2018, 57, 4430−4441

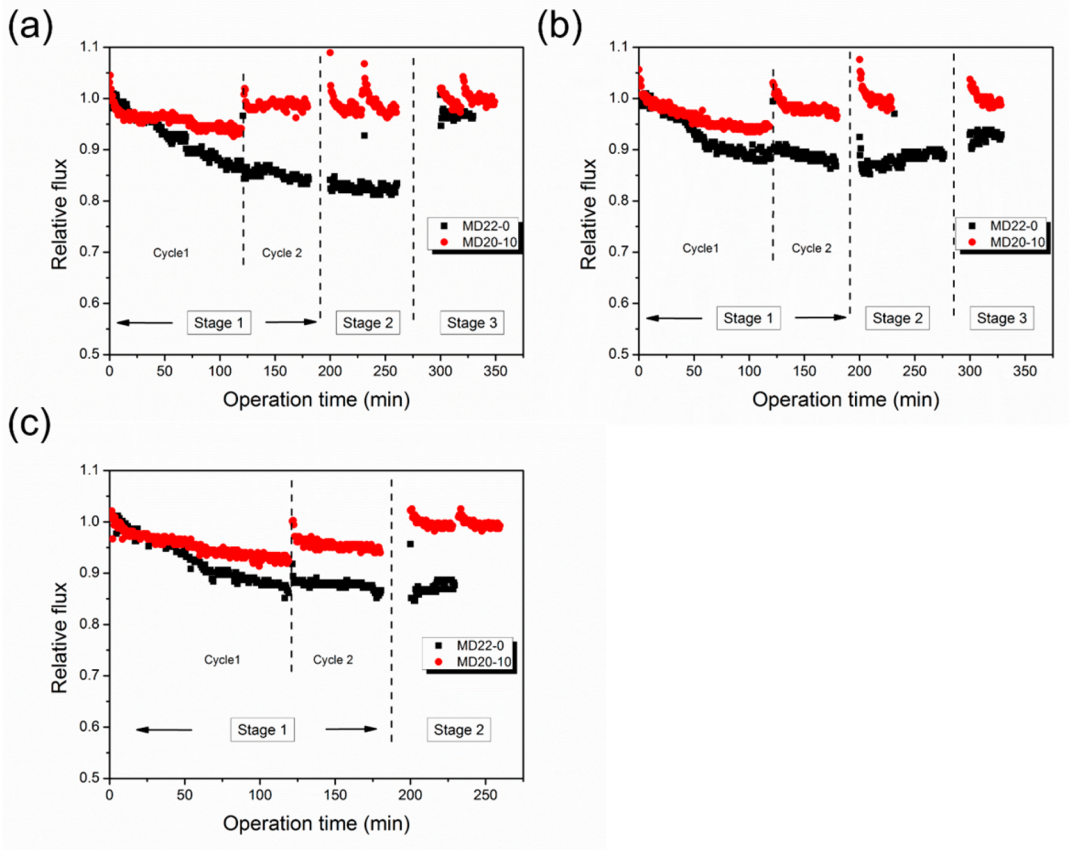

Figure 7. Flux change of full-size membrane modules (MD22-0 and MD20-10) by using real river water samples (a, Yodo River; b, Kako River; and c, Seta River).

During the BSA fouling measurement, initial water fluxes were set at the same level (approximately 20 L m^{-2} h^{-1}) by altering the operation pressure (25 kPa for MD22-0 and 44 kPa for MD20-10). The relative water flux of MD20-10 is approximately1.5 times as high as that of MD22-0 after 6 h of fouling test (Figure 5b). Also, FRRs for MD20-10 are stable at 87%, while those for MD22-0 decrease from 67% to 52% (Figure 5c). Another important thing should be highlighted that the accumulative volume after a 6 h test is 92 L m^{-2} for MD20-10 but that is only 47 L m^{-2} for MD22-0, and the accumulative volumes per operation pressure are 2.09 and 1.88 L m^{-2} kPa^{-1} for MD20-10 and MD22-0, respectively (Figure 5d). This proves that due to the improved antifouling properties of the PES/SPES membranes, the module (MD20-10) consumes less energy to generate the same volume of clean water. It can also be estimated that when prolonging the operation time, the pure PES membrane module suffers from the more severe fouling and thus results in lower efficiency for water production.

3.2.4. Antifouling Evaluation of Full-Size Membrane Modules by Using Real River Water Samples. To evaluate the practical application in water treatment field, real river water samples from Yodo River, Kako River, and Seta River, three local rivers in Kansai region of Japan, were used to confirm the antifouling properties of the full-size modules containing pure and blend hollow fiber membranes. The water quality of these river water samples measured by LC-OCD and EEM is shown in Table S2 and Figure 6. Table S2 shows the TOC concentration is relatively low (1−2 ppm) compared with our model foulant solutions (100 ppm). LC-OCD is a technique that classifies the natural organic matter (NOM) into biopolymers, humics, building blocks, neutrals, and acids, based on the sizes and chemical functions of the matters.[35] This technique indicated that most part of the NOM in river water is humics and building blocks[42] (Figure 6). According to EEM analysis, fulvic acid-like and humic acid-like substances (total, 75−80%) are the dominant part of the NOM in the river water, and the remaining matter is protein.

The operation process for evaluating antifouling properties of the membrane modules by river water samples is as follows. This process also included three stages. In the first 120 min (cycle 1 in stage 1), the river water, containing 27 L of river water sample and 7 L of tap water, was circulated in the evaluation system at a specific pressure (for MD20-10, the pressure was 43.5 kPa; for MD22-0, the pressure was 25 kPa) with a flow rate of 130 L h^{-1}. After that, the module was backflushed under the pressure of 40−45 kPa for 30 s and aerated for 10 s with a flow rate of 2.5 L min^{-1}, and finally, the residual solution (approximately 2 L) was discharged. Then in 121−180 min (cycle 2 in stage 1), the permeate solution was collected and the fresh river water was supplemented into the foulant solution tank with a flow rate of 200 mL min^{-1}. In stages 2 and 3, the process was the same as described in section 2.5.

Figure 7 shows the flux change of the membrane modules when using the three river water samples. Flux decrease of MD20-10 is less than that of MD22-0 in all three river water cases. After the first rinsing process of 120 min, the water recovery ratios for MD20-10 are almost 100% in all cases, but those are ∼91% for MD22-0. After 3 h of river water treatment, the flux retentions are approximately 97% for MD20-10, and those are approximately 86% for MD22-0. This strongly indicates

DOI: 10.1021/acs.iecr.8b00114
Ind. Eng. Chem. Res. 2018, 57, 4430−4441

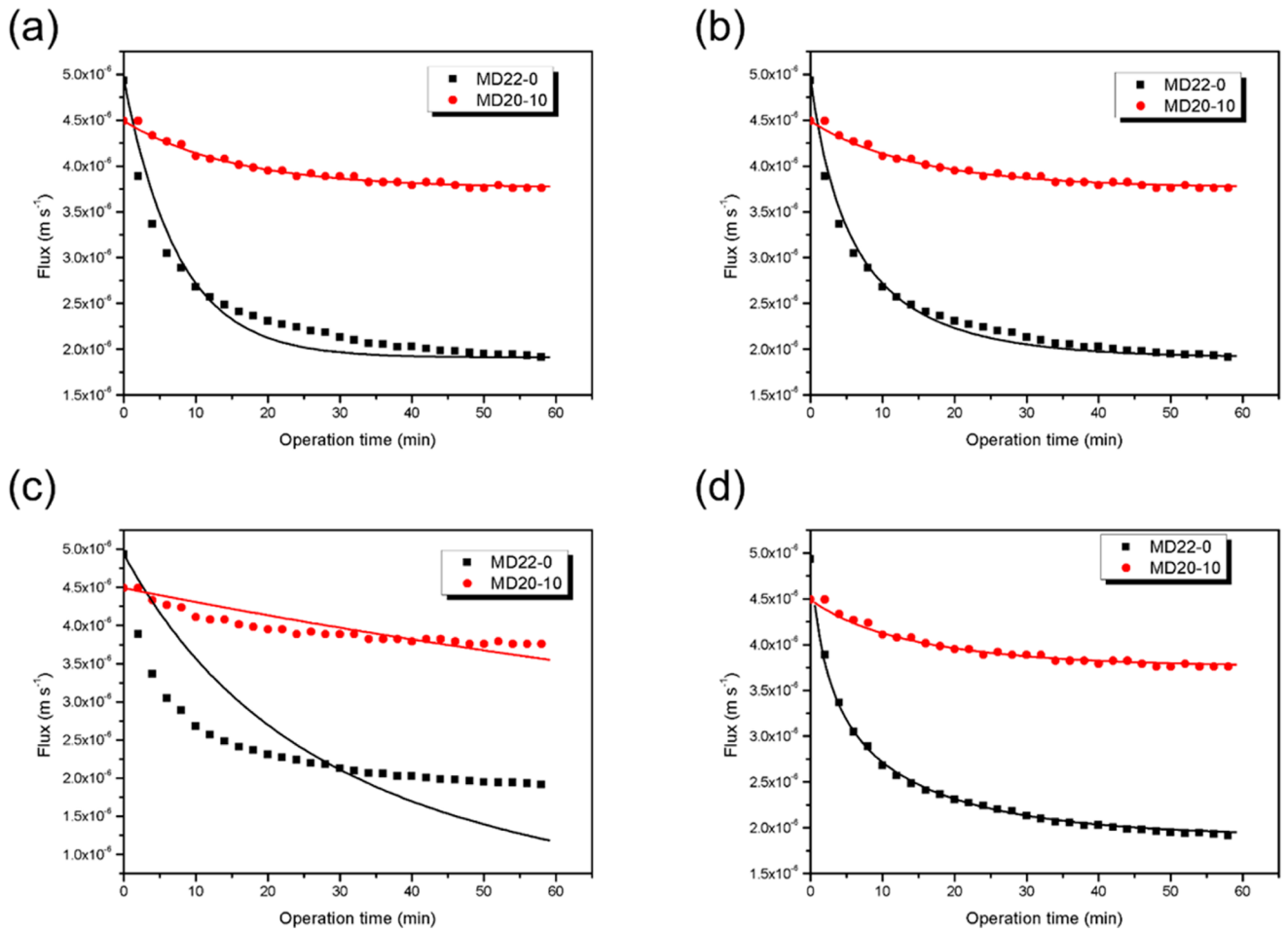

Figure 8. Complete blocking model (a), intermediate blocking model (b), standard blocking model (c), and gel layer formation model (d) for crossflow flux filtration predications for MD22-0 and MD20-10 using BSA as the model foulant. The inset black and red lines are model fitted lines.

that almost no membrane fouling occurs when MD20-10 is used. After the clean water rinsing process (stage 2), the flux is totally recovered for MD20-10, but it cannot be recovered for MD22-0, implying that the initial membrane fouling in MD22-0 is the irreversible fouling. Compared with the flux decrease observed in the model foulant solutions measurements, the fouling is much lower when using river water samples due to their low contaminant concentrations in the river water samples (Table S2). Therefore, MD20-10 exhibits better antifouling properties for real water treatment.

3.2.5. Chemical Cleaning of the Membrane Modules (Stage 3 Operation). Chemical cleaning is a facile and efficient approach to recover the membrane properties. In this study, NaClO/NaOH solution cleaning process was adopted to remove and degrade the contaminants in and/or on the membrane after one fouling measurement (Figures 4b, 5a, and 7a,b), and then the membrane modules were reused for the subsequent fouling experiments. In this case, the chemical cleaning was conducted by soaking the membranes modules in a 1000 ppm of NaClO and 1 mM NaOH solution for 3 days. According to the experimental results, the water permeability of MD20-10 in all cases was completely recovered, indicating that the membranes were recovered without breaking fibers. However, for MD22-0, the flux recovery ratios after chemical rinsing were approximately 70%, 90%, 95%, and 92%, when SA, HA, Yodo River water, and Kako River water were used as foulants, respectively. Therefore, the membrane module (MD20-10) with PES/SPES blend hollow fiber membranes is more easily cleaned and recovered by the chemical cleaning procedure, and this also proves that the chemical cleaning extent is sufficient for its practical application.

3.3. Fouling Modeling Fitting. To better understanding of the detailed fouling procedure of membrane modules during water treatment, Hermia's model was adopted to fit the flux. The general equation for Hermia's models adapted to crossflow ultrafiltration is shown as follows:[43]

$$-\frac{dJ}{dt} = K(J - J_{ss})J^{2-n} \tag{3}$$

where J is the permeate flux (m s^{-1}), K is a model constant, t is the filtration time (s), and J_{ss} is the steady-state flux during filtration (m s^{-1}). The parameter n is specific to fouling mechanisms according to Vela et al.,[34] and the detailed relationship between n and fouling mechanism is listed in Table S4.[34,44]

According to these four types of fouling model, the flux data (mainly the first cycle of filtration procedure) were fitted, and all the fitting data are listed in Figure 8, Figures S2–S6, Table 4, and Table S5. Generally, the filtration data can be well fitted by complete blocking model, intermediate blocking model, and gel layer formation model except the standard blocking model. According to the definition, when the size of solute molecules is greater than that of the membrane pores, the complete blocking occurs; while the solute molecule size is similar to the membrane

DOI: 10.1021/acs.iecr.8b00114
Ind. Eng. Chem. Res. 2018, 57, 4430–4441

Table 4. Fitted Hermia's Model Parameters

module	foulant	K_c (m^{-1})	K_i (m^{-1})	$K_s \times 10^3$ ($s^{-0.5}$ $m^{-0.5}$)	$K_{gl} \times 10^{-6}$ (s m^{-2})
MD22-0	SA	126.3	154.0	37.5	34.2
MD20-10	SA	120.5	129.7	13.6	26.2
MD22-0[a]	HA	226.7	238.3	8.2	49.5
MD20-10[a]	HA	132.8	137.2	5.4	24.8
MD22-0	BSA	446.7	631.7	132.2	255.0
MD20-10	BSA	241.7	260.0	16.6	66.7
MD22-0	Yodo	55.0	59.2	6.1	10.4
MD20-10	Yodo	63.3	64.8	1.9	11.2
MD22-0	Kako	55.2	58.7	5.4	10.6
MD20-10	Kako	91.7	95.2	3.2	16.4
MD22-0	Seta	53.7	57.3	5.9	11.0
MD20-10	Seta	42.3	43.3	2.0	7.6

[a]The fitted data is the fourth cycle data during filtration, because the initial water flux is fixed at the similar level for the modules by regulating the operation pressure in the fourth cycle.

pore size, the intermediate blocking occurs.[33,34] For gel layer formation, the solute molecules are greater than the membrane pores and do not penetrate inside them. Then the solutes deposit on the membrane surface and on the previously deposited solute layer.[33] When BSA and HA are used as the foulant, the rejections are higher than 80%, which means that most foulants are successfully retained by the membranes. Therefore, only the standard blocking model in which the foulant deposited inside the pores cannot fit well with the experimental data.

Furthermore, it can be found that the constant in fouling models (K_c, K_i, and K_{gl}) are dependent on the filtration system, and the values vary with membrane modules and the types of the foulant (Table 4). Especially, the constant (K_c, K_i, and K_{gl}) for MD20-10 using HA and BSA as the foulant is much lower that for MD22-0, implying the improved antifouling properties, while the constant (K_c, K_i, and K_{gl}) for MD20-10 using SA as the foulant is comparable to that for MD22-0. It may be caused by the properties of SA, which easily aggregates and become gel during filtration[45,46] and does not matter with the properties of the membranes. However, properties of the blend membrane are more easily recovered by back flushing compared with the pure PES membranes (Figure 4b). Moreover, due to the lower solute concentrations in real river water samples, the values of K (K_c, K_i, and K_{gl}) are much lower than those for model foulant solutions.

In this study, the values of K (K_c, K_i, and K_{gl}) are much larger than those in previous report using poly(ethylene glycol) (PEG) as model foulant.[34] One reason is probably caused by the different interactions between the membrane surface and the foulant. Compared with the model foulant (i.e., SA, HA, and BSA), the interaction between the foulant and the membrane surface is much stronger than that between PEG and membrane surface. Another reason is the different crossflow velocity during ultrafiltration process. In this work, the crossflow velocity is approximately 0.06 m s^{-1} for all modules during measurement, which is much lower than those in previous research (i.e., 1, 2, and 3 m s^{-1}). Therefore, for further improvement of antifouling properties of the membrane modules, increasing the crossflow velocity is an effective way.

From above fitting analysis, it can be concluded that the fouling mechanism of the membrane modules during ultrafiltration is complete blocking model, intermediate blocking model, or gel layer formation model, and the membrane module with PES/SPES blend membranes exhibits the better antifouling properties compared with the module with pure PES membranes.

4. CONCLUSIONS

In this study, a series of full-size membrane modules containing pure PES hollow fiber membranes and PES/SPES blend hollow fiber membranes were successfully fabricated. This is the first work that an evaluation of the antifouling properties of this type of blend membranes is carried out in the full-size membrane modules. From a comparison of the mechanical strength and antifouling properties of the blend membranes with different SPES fractions, the blend membranes with 10% SPES showed the best performance. By using SA, HA, and BSA as the model foulants, the improved antifouling properties of the membrane module containing the hollow fiber membranes with 10% of SPES (MD20-10) were confirmed. Moreover, flux decrease of MD20-10 was much lower than that of the membrane module containing pure PES membranes (MD22-0) during real river water filtration, also evidencing the improved properties of MD20-10. The module fouling analysis using Hermia's model confirmed that the main fouling mechanism involved the complete blocking model, intermediate blocking model, or gel layer formation model. A sufficient extent of chemical cleaning of MD20-10 was also confirmed, which implied a promising potential for its practical application.

■ ASSOCIATED CONTENT

Supporting Information

The Supporting Information is available free of charge on the ACS Publications website at DOI: 10.1021/acs.iecr.8b00114.

The sectional view of the nozzle; complete blocking model, intermediate blocking model, standard blocking model, and gel layer formation model for crossflow flux filtration predications for MD22-0 and MD20-10 using SA, HA, Yodo river water, Kako river water, and Seta river water as the foulants; summary of the reported hollow fiber modules in the literatures and the modules in this study; water qualities of three river water samples; compositions of the casting solutions for pure PES membranes and PES/SPES blend membranes; summary of the four fouling mechanism models; models fitting accuracy for the ultrafiltration of SA solution, HA solution, BSA solution, and real river water samples: values of R^2 (PDF)

■ AUTHOR INFORMATION

Corresponding Author

*E-mail: matuyama@kobe-u.ac.jp (H.M.).

ORCID

Hideto Matsuyama: 0000-0003-2468-4905

Notes

The authors declare no competing financial interest.

■ ACKNOWLEDGMENTS

This research was funded by a grant from the Ministry of Education, Culture, Sports, Science and Technology (MEXT) for the Regional Innovation Strategy Support Program of Japan and Grants-in-Aid from the Special Coordination Funds for Promoting Science and Technology, Creation of Innovation Centers for Advanced Interdisciplinary Research Areas (In-

DOI: 10.1021/acs.iecr.8b00114
Ind. Eng. Chem. Res. 2018, 57, 4430−4441

novative Bioproduction, Kobe) from the Ministry of Education, Culture, Sports, Science and Technology, Japan.

REFERENCES

(1) Hester, J. F.; Banerjee, P.; Mayes, A. M. Preparation of protein-resistant surfaces on poly(vinylidene fluoride) membranes via surface segregation. *Macromolecules* **1999**, *32*, 1643−1650.
(2) Asatekin, A.; Menniti, A.; Kang, S.; Elimelech, M.; Morgenroth, E.; Mayes, A. M. Antifouling nanofiltration membranes for membrane bioreactors from self-assembling graft copolymers. *J. Membr. Sci.* **2006**, *285*, 81−89.
(3) Zhao, Y.-H.; Zhu, B.-K.; Kong, L.; Xu, Y.-Y. Improving hydrophilicity and protein resistance of poly(vinylidene fluoride) membranes by blending with amphiphilic hyperbranched-star polymer. *Langmuir* **2007**, *23*, 5779−5786.
(4) Fang, L.-F.; Jeon, S.; Kakihana, Y.; Kakehi, J.-i.; Zhu, B.-K.; Matsuyama, H.; Zhao, S. Improved antifouling properties of polyvinyl chloride blend membranes by novel phosphate based-zwitterionic polymer additive. *J. Membr. Sci.* **2017**, *528*, 326−335.
(5) Rahimpour, A.; Madaeni, S. S.; Ghorbani, S.; Shockravi, A.; Mansourpanah, Y. The influence of sulfonated polyethersulfone (SPES) on surface nano-morphology and performance of polyethersulfone (PES) membrane. *Appl. Surf. Sci.* **2010**, *256*, 1825−1831.
(6) Xu, Y.; Wang, M.; Ma, Z.; Gao, C. Electrochemical impedance spectroscopy analysis of sulfonated polyethersulfone nanofiltration membrane. *Desalination* **2011**, *271*, 29−33.
(7) Kim, I.; Choi, J.; Tak, T. Sulfonated polyethersulfone by heterogeneous method and its membrane performances. *J. Appl. Polym. Sci.* **1999**, *74*, 2046−2055.
(8) He, T.; Mulder, M.; Strathmann, H.; Wessling, M. Preparation of composite hollow fiber membranes: co-extrusion of hydrophilic coatings onto porous hydrophobic support structures. *J. Membr. Sci.* **2002**, *207*, 143−156.
(9) Chen, S.-H.; Yu, K.-C.; Lin, S.-S.; Chang, D.-J.; Liou, R. M. Pervaporation separation of water/ethanol mixture by sulfonated polysulfone membrane. *J. Membr. Sci.* **2001**, *183*, 29−36.
(10) Li, Y.; Chung, T. S. Highly selective sulfonated polyethersulfone (SPES)-based membranes with transition metal counterions for hydrogen recovery and natural gas separation. *J. Membr. Sci.* **2008**, *308*, 128−135.
(11) Devrim, Y.; Erkan, S.; Bac, N.; Eroğlu, I. Preparation and characterization of sulfonated polysulfone/titanium dioxide composite membranes for proton exchange membrane fuel cells. *Int. J. Hydrogen Energy* **2009**, *34*, 3467−3475.
(12) Lufrano, F.; Squadrito, G.; Patti, A.; Passalacqua, E. Sulfonated polysulfone as promising membranes for polymer electrolyte fuel cells. *J. Appl. Polym. Sci.* **2000**, *77*, 1250−1256.
(13) Fu, Y.-Z.; Manthiram, A. Synthesis and characterization of sulfonated polysulfone membranes for direct methanol fuel cells. *J. Power Sources* **2006**, *157*, 222−225.
(14) Li, L.; Wang, Y. Proton conducting composite membranes from sulfonated polyethersulfone Cardo and phosphotungstic acid for fuel cell application. *J. Power Sources* **2006**, *162*, 541−546.
(15) Rikukawa, M.; Sanui, K. Proton-conducting polymer electrolyte membranes based on hydrocarbon polymers. *Prog. Polym. Sci.* **2000**, *25*, 1463−1502.
(16) Dai, H.; Guan, R.; Li, C.; Liu, J. Development and characterization of sulfonated poly (ether sulfone) for proton exchange membrane materials. *Solid State Ionics* **2007**, *178*, 339−345.
(17) Shi, W.; He, B.; Li, J. Esterification of acidified oil with methanol by SPES/PES catalytic membrane. *Bioresour. Technol.* **2011**, *102*, 5389−5393.
(18) Shi, W.; He, B.; Cao, Y.; Li, J.; Yan, F.; Cui, Z.; Zou, Z.; Guo, S.; Qian, X. Continuous esterification to produce biodiesel by SPES/PES/NWF composite catalytic membrane in flow-through membrane reactor: experimental and kinetic studies. *Bioresour. Technol.* **2013**, *129*, 100−107.
(19) Fang, L.-F.; Yang, H.-Y.; Cheng, L.; Kato, N.; Jeon, S.; Takagi, R.; Matsuyama, H. Effect of Molecular Weight of Sulfonated Poly(ether sulfone) (SPES) on the Mechanical Strength and Antifouling Properties of Poly(ether sulfone)/SPES Blend Membranes. *Ind. Eng. Chem. Res.* **2017**, *56*, 11302−11311.
(20) Wang, H.; Yang, L.; Zhao, X.; Yu, T.; Du, Q. Improvement of Hydrophilicity and Blood Compatibility on Polyethersulfone Membrane by Blending Sulfonated Polyethersulfone. *Chin. J. Chem. Eng.* **2009**, *17*, 324−329.
(21) Li, Y.; Chung, T.-S. Exploration of highly sulfonated polyethersulfone (SPES) as a membrane material with the aid of dual-layer hollow fiber fabrication technology for protein separation. *J. Membr. Sci.* **2008**, *309*, 45−55.
(22) Cao, X.; Tang, M.; Liu, F.; Nie, Y.; Zhao, C. Immobilization of silver nanoparticles onto sulfonated polyethersulfone membranes as antibacterial materials. *Colloids Surf., B* **2010**, *81*, 555−562.
(23) Zhang, Y.; Feng, X.; Yuan, S.; Zhou, J.; Wang, B. Challenges and recent advances in MOF−polymer composite membranes for gas separation. *Inorg. Chem. Front.* **2016**, *3*, 896−909.
(24) Xiao, K.; Xu, Y.; Liang, S.; Lei, T.; Sun, J.; Wen, X.; Zhang, H.; Chen, C.; Huang, X. Engineering application of membrane bioreactor for wastewater treatment in China: Current state and future prospect. *Front. Environ. Sci. Eng.* **2014**, *8*, 805−819.
(25) Lang, W.-Z.; Xu, Z.-L.; Yang, H.; Tong, W. Preparation and characterization of PVDF−PFSA blend hollow fiber UF membrane. *J. Membr. Sci.* **2007**, *288*, 123−131.
(26) Qin, J.-J.; Oo, M. H.; Li, Y. Development of high flux polyethersulfone hollow fiber ultrafiltration membranes from a low critical solution temperature dope via hypochlorite treatment. *J. Membr. Sci.* **2005**, *247*, 137−142.
(27) Tan, X.; Tan, S.; Teo, W.; Li, K. Polyvinylidene fluoride (PVDF) hollow fibre membranes for ammonia removal from water. *J. Membr. Sci.* **2006**, *271*, 59−68.
(28) Wang, D.; Li, K.; Teo, W. Preparation and characterization of polyvinylidene fluoride (PVDF) hollow fiber membranes. *J. Membr. Sci.* **1999**, *163*, 211−220.
(29) Xu, Z.-L.; Qusay, F. A. Polyethersulfone (PES) hollow fiber ultrafiltration membranes prepared by PES/non-solvent/NMP solution. *J. Membr. Sci.* **2004**, *233*, 101−111.
(30) Yang, Q.; Chung, T.-S.; Weber, M. Microscopic behavior of polyvinylpyrrolidone hydrophilizing agents on phase inversion polyethersulfone hollow fiber membranes for hemofiltration. *J. Membr. Sci.* **2009**, *326*, 322−331.
(31) Yu, L.-Y.; Xu, Z.-L.; Shen, H.-M.; Yang, H. Preparation and characterization of PVDF−SiO 2 composite hollow fiber UF membrane by sol−gel method. *J. Membr. Sci.* **2009**, *337*, 257−265.
(32) http://www.toraywater.com/products/mf/Pressurized%20_HFUHFS_series.pdf; http://www.gelifesciences.com/webapp/wcs/stores/servlet/productById/en/GELifeSciences-us/39000000; http://www.kochmembrane.com/PDFs/Data-Sheets/Hollow-Fiber/UF/romipro-3-inch-hf-ctg-datasheet.aspx.
(33) Vela, M. C. V.; Blanco, S. Á.; García, J. L.; Rodríguez, E. B. Analysis of membrane pore blocking models applied to the ultrafiltration of PEG. *Sep. Purif. Technol.* **2008**, *62*, 489−498.
(34) Vincent Vela, M. C.; Álvarez Blanco, S.; Lora García, J.; Bergantiños Rodríguez, E. Analysis of membrane pore blocking models adapted to crossflow ultrafiltration in the ultrafiltration of PEG. *Chem. Eng. J.* **2009**, *149*, 232−241.
(35) Huber, S. A.; Balz, A.; Abert, M.; Pronk, W. Characterisation of aquatic humic and non-humic matter with size-exclusion chromatography−organic carbon detection−organic nitrogen detection (LC-OCD-OND). *Water Res.* **2011**, *45*, 879−885.
(36) Chen, W.; Westerhoff, P.; Leenheer, J. A.; Booksh, K. Fluorescence Excitation−Emission Matrix Regional Integration to Quantify Spectra for Dissolved Organic Matter. *Environ. Sci. Technol.* **2003**, *37*, 5701−5710.
(37) Susanto, H.; Ulbricht, M. Characteristics, performance and stability of polyethersulfone ultrafiltration membranes prepared by phase separation method using different macromolecular additives. *J. Membr. Sci.* **2009**, *327*, 125−135.

DOI: 10.1021/acs.iecr.8b00114
Ind. Eng. Chem. Res. 2018, 57, 4430−4441

(38) Yip, N. Y.; Tiraferri, A.; Phillip, W. A.; Schiffman, J. D.; Elimelech, M. High performance thin-film composite forward osmosis membrane. *Environ. Sci. Technol.* **2010**, *44*, 3812−3818.
(39) Tiraferri, A.; Yip, N. Y.; Phillip, W. A.; Schiffman, J. D.; Elimelech, M. Relating performance of thin-film composite forward osmosis membranes to support layer formation and structure. *J. Membr. Sci.* **2011**, *367*, 340−352.
(40) Fang, L.-F.; Zhu, B.-K.; Zhu, L.-P.; Matsuyama, H.; Zhao, S. Structures and antifouling properties of polyvinyl chloride/poly(methyl methacrylate)-graft-poly(ethylene glycol) blend membranes formed in different coagulation media. *J. Membr. Sci.* **2017**, *524*, 235−244.
(41) Zhu, L.; Liu, F.; Yu, X.; Xue, L. Poly(Lactic Acid) Hemodialysis Membranes with Poly(Lactic Acid)-*block*-Poly(2-Hydroxyethyl Methacrylate) Copolymer As Additive: Preparation, Characterization, and Performance. *ACS Appl. Mater. Interfaces* **2015**, *7*, 17748−17755.
(42) Kimura, K.; Tanaka, K.; Watanabe, Y. Microfiltration of different surface waters with/without coagulation: Clear correlations between membrane fouling and hydrophilic biopolymers. *Water Res.* **2014**, *49*, 434−443.
(43) Corbatón-Báguena, M.-J.; Álvarez-Blanco, S.; Vincent-Vela, M.-C. Fouling mechanisms of ultrafiltration membranes fouled with whey model solutions. *Desalination* **2015**, *360*, 87−96.
(44) Abbasi, M.; Taheri, A. Modeling of permeation flux decline during oily wastewaters treatment by MF-PAC hybrid process using mullite ceramic membranes. *Indian J. Chem. Technol.* **2014**, *21*, 49−55.
(45) Chen, K. L.; Mylon, S. E.; Elimelech, M. Aggregation Kinetics of Alginate-Coated Hematite Nanoparticles in Monovalent and Divalent Electrolytes. *Environ. Sci. Technol.* **2006**, *40*, 1516−1523.
(46) Katsoufidou, K.; Yiantsios, S. G.; Karabelas, A. J. Experimental study of ultrafiltration membrane fouling by sodium alginate and flux recovery by backwashing. *J. Membr. Sci.* **2007**, *300*, 137−146.

DOI: 10.1021/acs.iecr.8b00114
Ind. Eng. Chem. Res. 2018, 57, 4430−4441